

A Radio SETI Campaign for μ s-s Periodic Signals

Short title: SETI Autocorrelation Survey with ATA

G. R. Harp¹, R. F. Ackermann¹, Alfredo Astorga¹, Jack Arbunich¹, Jose Barrios¹, Kristin Hightower¹, Seth Meitzner¹, W. C. Barott², Michael C. Nolan³, D. G. Messerschmitt⁴, Douglas A. Vakoch¹, Seth Shostak¹, J. C. Tarter¹

¹ Center for SETI Research, SETI Institute, 189 Bernardo Ave., Ste. 100, Mountain View, CA, 94043.

² Electrical & System Engineering Dept., Embry-Riddle Aeronautical University, 600 S. Clyde Morris Blvd, Daytona Beach, FL, USA, 32114.

³ Arecibo Observatory, HC3 Box 53995, Arecibo, PR 00612, USA.

⁴ Department of Electrical Engineering and Computer Sciences, University of California at Berkeley, 387 Soda Hall, Berkeley, CA 94720-1776.

Abstract

We report a novel radio autocorrelation (AC) search for extraterrestrial intelligence (SETI). For selected frequencies across the terrestrial microwave window (1-10 GHz) observations were conducted at the Allen Telescope Array to identify artificial non-sinusoidal periodic signals with radio bandwidths greater than 4 Hz, which are capable of carrying substantial messages with symbol-rates from $4\text{-}10^6$ Hz. Out of 243 observations, about half (101) were directed toward sources with known continuum flux $> \sim 1$ Jy (quasars, pulsars, supernova remnants, and masers), based on the hypothesis that they might harbor heretofore undiscovered natural or artificial, repetitive, phase or frequency modulation. The rest of the targets were mostly toward exoplanet stars and similarly interesting targets from the standpoint of SETI. This campaign places constraints on previously untested hypotheses relating to the number of artificially modulated sources. No potential signals of extraterrestrial technology were found in this study. We conclude that the maximum probability that future observations like the ones described here will reveal repetitively modulated emissions from a wide variety of sources, including quasars, supernova remnants, and bright stars, is no more than 3-23 percent, depending on source type. The paper concludes by describing a new approach to expanding this survey to many more targets and much greater sensitivity using archived data from interferometers all over the world.

Keywords: astrobology; instrumentation: detectors; instrumentation: interferometers; methods; data analysis; radio continuum: general; quasars: general

1 Introduction

Searches for Extraterrestrial Intelligence (SETI) at radio frequencies traditionally focus on slowly modulated narrowband signals (Cocconi & Morrison 1959; Drake 1961; Oliver & Billingham 1971; Shuch 2011; Tarter 2001). The premise of the narrowband (~ 1 Hz) search is that relatively weak narrowband ETI signals may be present but hidden in ordinary astronomical observations.

One unspoken assumption is that all radio sources already known to astronomers have a natural origin. This paper recognizes that this statement is not fully supported by existing observations. Some well-known strong radio sources might harbor a hidden message masquerading as, or piggybacking on, a strong natural source. While many pulsars and other sources may have been previously tested for repetitive power modulation, the authors are not aware of previous work testing for encodings that use e.g. constant-power phase modulation from known bright sources. The latter is the focus here.

Suppose ET were to construct a powerful transmitter sending information at a bit rate between $10^3 - 10^9$ Hz. To most radio telescopes, such a transmitter is indistinguishable from a natural continuum source because the time fluctuations are too short to appear in standard detectors. However, these same signals can be detectable by autocorrelating the electric field amplitude and phase, otherwise known as a field autocorrelation (FAC) detection. Here we present what we believe to be the first radio search for ETI using FAC

detection of complex signals. As an alternative we also consider intensity autocorrelation for detection of incoherent amplitude modulated signals.

Recently there has been a resurgence of theoretical research on searching for *wideband* engineered signals that may be used for interstellar messaging (Ackermann & Harp 2012; Gardner & Spooner 1992; Harp et al. 2010a; Von Korff et al. 2013; Messerschmitt 2012; Messerschmitt & Morrison 2012; Morrison 2012, 2017; Siemion et al. 2010). Meanwhile, techniques developed for very long baseline interferometry have been adapted to capture substantial bandwidths (>1 MHz) of digitized time series data for post-processing (Harp et al. 2010a; Korpela et al. 2001; Morrison 2012; Siemion et al. 2010; Tarter et al. 2010; Wayth et al. 2011). The benefit of archiving such data is that they may be processed in ways that could not be performed in real time. This paper reports SETI observations that make use of this non-traditional approach.

1.1 Conventional Matched Filter Bank Searches and AC

Searches for narrowband continuous and pulse signals depend upon the assumption of preconceived signal types. The prototypal ET signal appears as a narrow sloping or slightly curved trace in a frequency vs. time spectrogram or waterfall plot (c.f. Figure 1). The intensity-inverted waterfalls of Figure 1 portray a narrowband signal from the ISEE3 spacecraft (left) and a dispersed pulse of radiation from the Crab pulsar (right). To highlight the similarity of the waterfalls, the space and frequency axes are swapped between left and right images. The ISEE3 signal is not vertically aligned because of the relative acceleration between spacecraft and detector. The pulse is similarly slanted for a different reason: Light propagation in the interstellar medium is dispersed (increasingly retarded at lower frequencies).

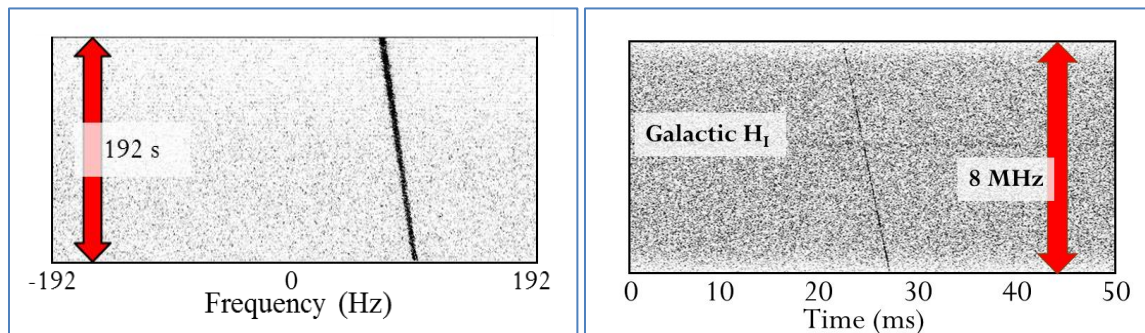


Figure 1: (Left) Time versus frequency waterfalls taken at ATA where the narrow dark trace indicates detection of a narrowband transmission from spacecraft ISEE3 during its closest approach to Earth. (Right) Frequency versus time waterfall where the trace indicates detection of one wideband “giant pulse” from the Crab pulsar. The horizontal line in the crab data corresponds to galactic HI emission at 1420 MHz.

Searches for such signals look for modestly curved traces in the time-frequency domain having small perpendicular cross-section (width \ll cross-width¹). Such searches can be

¹ The variables length l and width w require a definition of units to be compared. One way of consistently defining units is to measure l in units of the inverse width w^{-1} . On the left side of Figure 1, $w \sim 5$ Hz implying a time unit of 0.2 s, hence $l \sim 192 / 0.2 = 960$ time units perpendicular to w . On the right side,

parameterized with 2 to 3 independent parameters: the frequency f , slope or drift rate df/dt , and sometimes curvature or d^2f/dt^2 . In an equivalent pulse search, the time and frequency are swapped: $t, dt/df, d^2t/df^2$.²

Signals are detected using a matched filter bank (MFB) which effectively prepares a set of test waveforms spanning the parameter ranges and compares them to the observed waveform. Unfortunately, computation time for a parameterized MFB does not scale well, increasing geometrically with the number of parameters. For this reason, most modern SETI searches probe restricted parameter ranges of search coefficients for parameters and their first derivatives only. Matched filtering against additional parameters is too time-consuming to pursue systematically. The benefit of MFBs is their sensitivity. Historically it has been argued that it is better to search a narrow signal space with the greatest sensitivity than to search widely with moderate sensitivity (Oliver & Billingham 1971).

In this campaign, we use AC detection rather than an MFB. The search philosophy is that we wish to maximize the product of two factors:

1. A factor N_{Types} that measures the number of different signal types probed in a given search.
2. A factor N_{Stars} which measures the number of stars from which signal detection is possible given a fixed ET transmitter power and ATA's detection sensitivity.

We shall see below that AC detection of weak artificial signals is less sensitive (requires stronger transmitters) than MFB detection. Yet the number of signal types probed is astronomically larger, tilting the figure of merit $N_{\text{Stars}}N_{\text{Types}}$ in favor of AC over MFB when computation resources are limited.³ We shall argue that it makes sense to implement all of total power, narrowband and FAC detectors for future SETI observations, especially when observing with radio interferometers.

1.2 Research Hypotheses

To summarize, this observational campaign tests the following hypotheses (with more detail to be found in the discussion section):

- Hypothesis 1.** The emitted electric fields of most previously discovered strong radio sources with flux >1 Jy are modulated with a repeating pattern either directly by extraterrestrials or due to some heretofore unknown physics.

$w \sim 0.2$ s implies a frequency unit of 5, and $l = 8 \times 10^6 / 5 = 2 \times 10^5$. In both cases, $w \ll l$ is satisfied, which is the working definition of a "trace" in a waterfall.

² In practice, a fast search for naturally dispersed pulses can take advantage of the fact that the second and third parameters are co-dependent thus requiring only a 2 parameter matched filter bank in the search (Zackay, B. & Ofek, E. O. 2012).

³ Other figures of merit may result in different conclusions.

Hypothesis 2. Most bright pulsars, besides their characteristic repetitive nature, are additionally modulated as above.

Hypothesis 3. Out of all the stars in the galaxy, most harbor repeating transmitters.

We emphasize that to the best of our knowledge these hypotheses cannot be excluded from past observations over repetition periods considered here. This is the first substantial FAC ETI search for phase or frequency modulated repetitive signals. We also explore the utility of another detector, intensity autocorrelation as described in Section 2.

Besides the source types mentioned above, this campaign includes a small number of targets with special interest for SETI such as the galactic anti-center and the Earth-Sun Lagrange L4 point, and many reference observations used as comparators for testing the direction of origin of newly detected candidate signals.

The rest of this paper contains a description of the ETI signal detection techniques used here along with sensitivity calculations and comparisons to traditional matched filtering. Within this discussion we introduce the details of the observations, followed by a few examples of newly discovered technological signals. A discussion section summarizes the results and extracts quantitative results. This is followed by a brief demonstration of how repetitive signals can be detected in typical radio interferometer images and how this research can be extended to the analysis of large libraries of archived radio interferometer data.

2 Signal Detection Algorithms

Autocorrelation-based detection strategies can be a powerful addition to the toolkit of the traditional SETI narrowband search. Autocorrelation 1) is sensitive to a wide class of signals that are not effectively detected in a narrowband search, 2) has the potential for detecting signals containing messages with substantial information rates, and 3) is insensitive to dispersion in the interstellar medium (Harp et al. 2010a). The last is critical since wideband radio signals are strongly dispersed in the interstellar medium.

We demonstrate this immunity to dispersion with a simulation. We model a distant transmitter emitting four short pulses of sinusoidal radiation at 1 GHz and emitted over a period of 4000 seconds as in Figure 2 left (solid line). After traveling 1600 light years through a plasma with mean electron density equal to that of the galactic interstellar medium ($0.01 \text{ e}^- \text{ cm}^{-3}$), the dispersion measure (DM) of the signals will be about 5 pc cm^{-3} . Applying the well-known formula for cold plasma dispersion, an estimate of the dispersion measure is (Cordes 2002) $\text{delay (s)} = 0.00415 \text{ DM} / f^2 (\text{GHz})$. We calculate the pulse (electric field) amplitudes as they would appear at the receiver, Figure 2, left (dots). On the right-hand side of Figure 2, we display the complex-valued field autocorrelation (FAC, algorithm defined below) of the received signal with itself (line). As expected, the FAC detector shows 6 spikes for the original 4 pulses (zero delay spike has been suppressed). FAC is compared to the intensity autocorrelation (IAC, defined below).

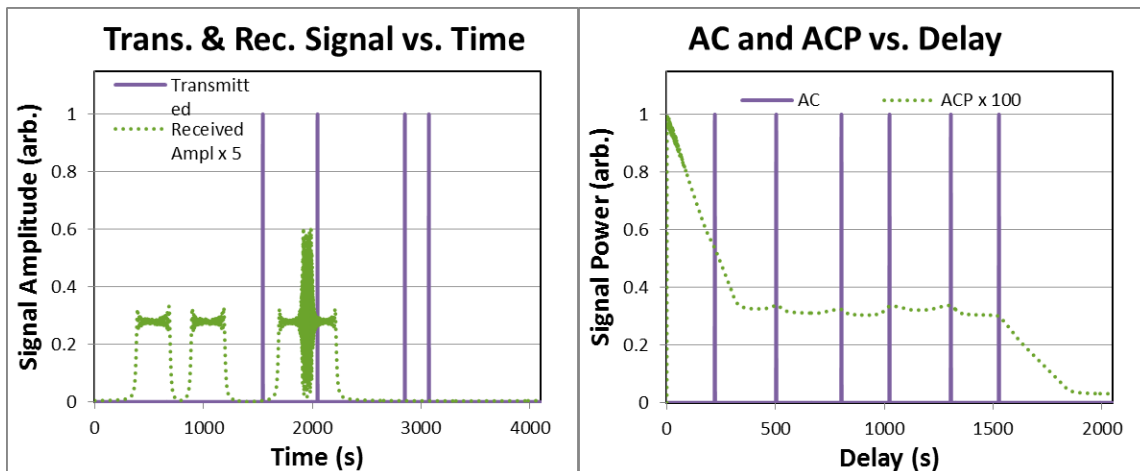


Figure 2: Transmission and reception of a coherent pulsed signal after passage through the interstellar medium for 1600 years. The left graph compares a baseband copy of the transmitted electric field amplitude at the transmitter (solid line) and receiver (dots). On the right we plot the autocorrelation of the received electric field (FAC, line) and autocorrelation of intensity (IAC, dots) for the signal. The repetitive signal is detectable in both FAC and IAC.

The example of Figure 2 visualizes a more general result: An FAC filter detects a coherent⁴ repetitive signal passed through any stationary linear filter just the same as if the data are not filtered. Hence FAC is immune not only to dispersion but also resistant to the effects of slowly varying scintillation (timescales longer than observation period) in the interstellar medium.

FAC discriminates between natural and engineered signals. For the engineered coherent pulses modeled in Figure 2, FAC discrimination (height of peaks compared to surrounding values) is generally quite good provided the received signal has a sufficient signal to noise ratio (see below). By comparison, known emission processes for e.g. pulsars and quasars give rise to phase incoherent signals which would not be detected with FAC. This is why FAC is not used for pulsar searches. As far as we know, only artificial, engineered processes can give rise to signals detectable in FAC.

The coherent FAC process used here is not ordinarily accessible for astronomy at optical frequencies, which usually measures only intensities. Intensity autocorrelation is the extension of FAC methods to light curves. Intensity autocorrelation finds application in many areas of physics, such as characterization of ultra-short optical pulses, the detection of weak optical pulsars (Leeb et al. 2015), interstellar scintillation of quasars (Rickett et al. 2002), and measuring stellar rotation periods from Kepler light curve data (McQuillan et al. 2014).

Incoherent signals can be detected by intensity autocorrelation (IAC) even when FAC fails to find them. IAC is closely related to the method of synchronous averaging of power used in pulsar searches. While the basic principles behind IAC are not new in radio astronomy, we describe this method here as a comparison to FAC.

⁴ In this discussion, “coherent” pulses are defined as having strong correlation between separate pulses. That is, pulses in the train have electric field waveform.

2.1 Signal Types

In SETI searches at the ATA we identify a few archetypal quasi-stationary signal waveforms:

- (A) *Narrowband*: A nearly-sinusoidal signal where the coherence time is of order 100 ms or longer. In the workhorse implementation at the ATA, called SonATA, such signals may carry up to 10 bits/s of information. We refer to this method as “conventional SETI.”
- (B) *Wideband power detection*: With an interferometer like the ATA, it is straightforward to capture “snapshots” of the sky, covering many square degrees. These snapshots can be compared across time periods from seconds to hours, or even longer. Such power intensity images may be examined for point sources that could be associated with ET transmitters or other unexpected radiation.
- (C) *Cyclostationary*: A finite alphabet of radio waveforms representing symbols is transmitted resulting in repetitions at specific delays when the same symbol is repeated. This mode is often used in satellite communication implementing error correction (Gardner & Spooner 1992; Leshem et al. 2000; Morrison 2012, 2011). Message information might be encoded in the transmission center frequency, time delay or signal phase. When substantial galactic dispersion is present, such symbols will generally overlap in time (c.f. dispersed pulses in Figure 2) which significantly impacts signal discovery in IAC but has little impact on signal detectability with FAC unless the repetition period is longer than the inverse Doppler drift rate $(df / dt)^{-1}$ of the transmitter relative to the receiver.

With phase modulation, an alphabet may be constructed from a single symbol multiplied by an overall phase factor. With such alphabets, all symbols correlate with all other symbols (see e.g. GPS example in (Harp et al. 2010a)). However, destructive interference between correlations of different symbol pairs can dilute FAC sensitivity. A solution to this problem is described in (Morrison 2012), but we do not adopt it here because it is computationally unfeasible at this time.

As the number of symbols in the alphabet grows, FAC sensitivity is also diluted since the average density of like symbols is reduced. This effect does not substantially alter the conclusions of this paper.

On Earth, cyclostationary signals which contain no extrinsic information (same symbol repeated over and over) are sometimes used in radar applications (e.g. Arecibo planetary radar) to generate a controlled wide bandwidth signal. If such a signal were discovered in SETI, it would still be conspicuously artificial and of interest.

(D) *Amplitude Modulation (AM)*:

- a) *Direct transmission*, as with broadcast radio. AM is more prone to errors caused by noise and fading than frequency or phase modulation.
- b) *Receive, delay and transmit (RDT)*: One suggestion is that ET may take advantage of a strong natural source to enhance detectability. For example, ET can set up a transmitter on a line of sight between Earth and a quasar. ET collects the quasar signal, amplifies it, and re-transmits a delayed copy toward Earth (Harp et al. 2010a). Information may be embedded in such a signal using a time-dependent delay.
- c) *Source modulation*: Direct amplitude modulation of an astronomical source might be accomplished by modulating or pumping the source itself. As proof of the principle, (Weisberg et al. 2005) has identified a maser source that is modulated by a pulsar. Since the light crossing time of the smallest masers is on the order of hundreds of seconds (Boyd & Werner 1972) modulations at shorter timescales indicate a localized pumping source.
- d) *Other*: The signal modulations above assume that the received signal is approximately stationary over time periods on the order of 100 ms or smaller. Of course, an infinity of other signal types exist including non-stationary signals that might be picked up with our autocorrelation detectors below. This is not a problem since any signal we find has a high likelihood of being artificial.

2.2 Sensitivity of Various Detectors

We consider a single polarization system where the telescope voltages are digitally sampled and a total of N_s samples are gathered in the observation. The total power P_t for a 1σ detection of a signal is proportional to the telescope's system equivalent flux density (SEFD), that is when the astronomical flux density is equal to the system noise power. More precisely,

$$P_t = \frac{(\text{SEFD})}{\sqrt{N_s}}, \quad \text{where} \quad \text{SEFD} = \frac{2\eta k_B T_{\text{sys}}}{\eta_{\text{eff}} A}, \quad (1)$$

and $\eta < 1$ is the power loss factor associated with digitization, k_B is Boltzmann's constant, A is the total collecting area and $\eta_{\text{eff}} < 1$ is aperture efficiency, or the fraction of A that is captured by the receiver in the combined optical system. At the ATA, $\eta_{\text{eff}} = 0.6$ (Harp et al. 2011). For equal signal in two polarizations, P_t is divided by $\sqrt{2}$.

Using measured antenna system temperatures, Table 1 displays the computed sensitivity measures for the various detection algorithms. At four frequencies used in observations, the measured ATA system temperature⁵ is used to compute the SNR for a 10-minute observation of a 1 Jy source (e.g. ETI transmitter or a quasar) emitting uniformly over the

⁵ New receivers are presently being installed at ATA which have lower system temperatures are currently being installed at ATA, but these were not available during the epoch of this work.

7 MHz detector bandwidth in column 3. The 4th column shows the flux of a source detectable at 1σ for a total-power measurement of a wideband signal. For a narrowband signal, column 5 shows the minimum detectable flux in a 1 Hz bin. Using FAC and IAC detectors and under the most favorable conditions (Fano 1951), column 6 applies.

Table 1:

Detection Thresholds for Various Algorithms
Assumes 600 s at 7 MHz bandwidth, $A_{eff} = 438 \text{ m}^2$.

f (GHz)	T_{sys} (K)	SNR 1 Jy Source	1σ Wideband Detectable Flux (Jy)	1σ Narrowband Detectable Flux in 1 Hz bin (Jy)	1σ FAC, Detectable Flux (Jy)
1.43	80	129	0.009	27	0.037
3.04	120	86	0.014	40	0.054
6.667	95	108	0.011	32	0.043
8.4	137	75	0.016	45	0.063

The 4th column in Table 1 shows the power detection threshold for a signal whose bandwidth $BW_{signal} \geq BW_{detector}$. The analogous detection threshold for a very narrowband signal is larger by a factor of $\sqrt{N_{chan}}$, where N_{chan} is the number of channels across the detector bandwidth. This is because all the power in the threshold wideband signal must be transmitted in a single channel. The detection thresholds for a 1 Hz bandwidth signal are shown in column 5 of Table 1 for reference only. When comparing sensitivities of different detectors, column 4 is the relevant column for an arbitrary MFB irrespective of the actual transmitted signal bandwidth.

The sixth column shows the detection sensitivity of the FAC and IAC. The most relevant comparison for column 6 is column 4. We return to this comparison in the discussion section.

This paper focuses on FAC as an alternative to the narrow band search for ETI. In the next section we describe FAC predict its relative sensitivities.

2.3 Two Alternative Detectors

The two detectors FAC and IAC mentioned above are introduced with notional expressions for their computation as compared with that for the traditional power spectrum (PS). The actual digital calculations require subtle corrections that are described in the Appendix. For the given observation time the number N_s of digitized samples are broken into N_b equal blocks of length M . Each block is processed with a Fourier transform (FT), which is then averaged over all blocks:

$$PS(f) = \sum_{n=0}^{N_b-1} \left| \sum_{m=0}^{M-1} \exp(-i 2\pi f t_m) s(nT + t_m) \right|^2 \quad (2)$$

$$FAC(\tau) = \sigma_s^{-2} \left| \sum_{l=0}^{M-1} \exp(i 2\pi f_l \tau) \sum_{n=0}^{N_b-1} \left| \sum_{m=0}^{M-1} \exp(-i 2\pi f_l t_m) s(nT + t_m) \right| \right| \quad (3)$$

$$IAC(\tau) = \sigma_{s^2}^{-2} \sum_{l=0}^{M-1} \exp(i 2\pi f_l \tau) \sum_{n=0}^{N_b-1} \left| \sum_{m=0}^{M-1} \exp(-i 2\pi f_l t_m) |s(nT + t_m)|^2 \right| \quad (4)$$

In Eqs. (2)-(4), $s(nT + t_m)$ is the value of the sample at point m in the n^{th} block, t_m is the time associated with s measured from the start of the n^{th} block, f_i is the baseband frequency, τ is the time delay measured from the start of the n^{th} block and σ_s^2 and $\sigma_{s^2}^2$ are the respective mean square variances of the field and intensity. These equations define the power spectrum (PS), averaged magnitude of sampled field autocorrelation (FAC), and averaged magnitude of sampled intensity autocorrelation (IAC) detectors, in that order (note squaring operation inside FT for IAC). As shown, the AC algorithms are implemented using the Wiener-Khinchin convolution theorem (Wozencraft & Jacobs, 1990 p. 73) with forward and inverse Fourier transforms. The units of PS and FAC are power, while IAC is different. With IAC, the fluctuations of the measured power are the “signal” we wish to characterize. The units of IAC are power also, based on this definition of “signal.”

PS uses an ordinary narrowband filter bank and this statistic represents a typical MFB detector.⁶ The FAC detector is sensitive to repeating modulations of the electric field. The IAC detector is sensitive to repeating modulations of the received power. Using FAC, amplitude modulation or constant amplitude signals with phase modulation or frequency modulation are detectable. IAC is sensitive to frequency and amplitude modulation but not constant-amplitude (e.g. phase) modulation. Comparatively, typical CCD detectors for light measure only the received power, after which IAC processing is sometimes possible. Radio measurements are special in that the phase of the electric field can be measured, permitting FAC detection.

In application we apply a simple 5σ threshold to the FAC statistic to identify signals that are likely to be engineered. Detection is done by visual inspection of graphs. As a function of frequency, approximate 1σ threshold flux values for detection are given in Table 1.

⁶ In actual observations, signals that deviate slightly from pure sinusoids are also checked.

2.4 Observational Design

The ATA is a dual-polarization 42-element interferometer located in Northern California, comprising 6.1 m dishes, dual-linear polarization feeds that operate in 4 simultaneous frequency bands centered anywhere between 1-10 GHz (Welch et al. 2009).

The signals from many ATA antennas are delayed and summed in a beam former (Barott et al. 2011). Complex-valued (8-bit real, 8-bit imaginary, hence $\eta \approx 1$) samples from the beam former are collected at a rate of 8.73 MS/s. An anti-aliasing bandpass filter before the digitizers limits the effective bandwidth to 7 MHz. The phased array beam diameter can be estimated as $0.1^\circ / f$, where f is the observation frequency in GHz. Quasars are effectively point-sources for the ATA and many are more than 100 times more powerful than the background level in the time period over which we perform FAC.

Data collections were made over approximately 14 months (Jan. 2010 – Mar. 2011). The typical ATA configuration used 25 of the 6.1 m antennas in a phased array beam on the source of interest. We accumulated data for typically 600 s, for an effective total of $N_s = 4.2 \times 10^9$ samples per observation. Referring to Equation (3), $M = 2^{23}$ or approximately 1 second long. The sampled data from each observation were reduced using Gnu Octave (Eaton et al. 1997) to compute the various statistics.⁷ All the source data are freely available on the internet (Harp et al. 2010b). Plots of PS and IAC were also generated for reference, but not included in the analysis here since those detectors have been well characterized before.

Many source targets (69) were chosen because they are known to have fluxes > 1 Jy. From Table 1 we see that if the entirety of that flux were repetitively modulated, then it would appear with high signal to noise in this survey. Additionally, sources for examination were chosen as follows: Exoplanets and Kepler objects of interest (59). Observations of 13 pulsars and the galactic anti-center were performed based on the hypothesis that ET might broadcast in the direction opposed to a known source in their field of view as an aid for our detection of them. Two strong methanol masers were observed to see if those masers might be artificially modulated. Six O type stars were chosen to study the hypothesis that advanced extraterrestrials might set up beacons using bright stars as an energy source. Other special pointings include the sun and moon for artifact tests, the Earth-Sun Lagrange L4 point (where transmitters might be left in a stable orbit), and the ecliptic North Pole.

Observational frequency bands were selected to have minimal strong radio frequency interference (RFI) and often encompass certain "magic" frequencies such as the $H_{1\alpha}$ line (1.420 GHz), $\sqrt{2} H_{1\alpha}$ (2.008 GHz), $2 H_{1\alpha}$ (2.840 GHz), $\pi H_{1\alpha}$ (4.462 GHz), the methanol maser line (6.667 GHz) and 8.4 GHz because it is close to the upper limit of ATA's receivers.

⁷ Source codes available upon request.

Only positive delays were examined since the curves are symmetric about zero delay.

Inspection was performed over the delay range $1 \times 10^{-4} < \tau < 0.25$ s, where the bias due to finite M is limited to no more than a factor of 2. The lower value is chosen to exclude features due to delays in time of arrival at different antennas in the ATA. The time spacing between plotted delays is the same as for the original sampling $\Delta\tau = 1.4 \times 10^{-7}$ s.

Interesting signals were noted and if those signals appeared in spectra from more than one pointing, they were identified as a ground or space-based man-made source.

2.5 Identification and Elimination of Human-Generated Signals

It is the goal of this paper to focus attention on detecting artificial (i.e. technological) signals no matter how they are generated. We wish to avoid the tedious work of identifying signals' specific transmitters, be they radar, cell phone, satellite, etc. Instead, we use direction of arrival methods to classify signals as either coming from the vicinity of Earth or coming from further away. Using these methods we can reliably eliminate signals from human transmitters out to about 10% of the orbit of the moon without any prior knowledge of spectrum usage. This is important since there is no part of the radio spectrum free from human interference. Since public documentation regarding most transmitters is spotty at best, it is impossible to rule out most signals out by any means other than direction of arrival.

3 Results

We demonstrate the utility of FAC detection with a few examples of (interfering) signals detected in this survey in Figure 3. Figure 3A shows a fiducial observation taken in the direction of a known spacecraft beyond lunar orbit (Deep Impact) in the frequency range of its communication downlink. This 35 Jy signal⁸ is exactly the type of signal we hope to observe. Plots B and C show an example of an unidentified 7 Jy signal that appeared in multiple pointings, hence identified as interference. Plot D shows how transmission from strong satellites (in this case Geostationary Operational Environmental Satellites or GOES) generate interfering signals at 3 Jy even when the telescope is not pointed at them. Plot E shows another unidentified 2 Jy signal which we labeled as interference because we deem it unlikely that an extraterrestrial transmitter would coincidentally repeat at such a round number (10.000 ms) in Earth units (also seen in more than one direction). Plot F shows a weak unidentified signal near the left-hand side with power at our 5σ detection limit (0.32 Jy for this frequency). This signal was observed in multiple pointing directions.

Taking a closer look, the signal in Plots B and C occurs right in the so-called protected radio astronomy band for the H_1 line. This signal was not visible in IAC, indicating that

⁸ Effective flux if spread over full 7 MHz bandwidth of our observations, computed with Table 1: and cross checked against an earlier DSN measurement
https://descanso.jpl.nasa.gov/DPSummary/di_article_cmp20050922.pdf.

it is probably phase-modulated. The FAC signal was observed in 7 MHz bands from 1400-1470 MHz with approximately uniform power. From this it is easy to understand why there was no detectable feature in the power spectrum (PS) for this signal. Also, because the source of this signal does not resolve to a point on the sky, even a repetitive signal as strong as this is not easily detected in ordinary interferometer observations and went undetected at the ATA for nearly a decade.

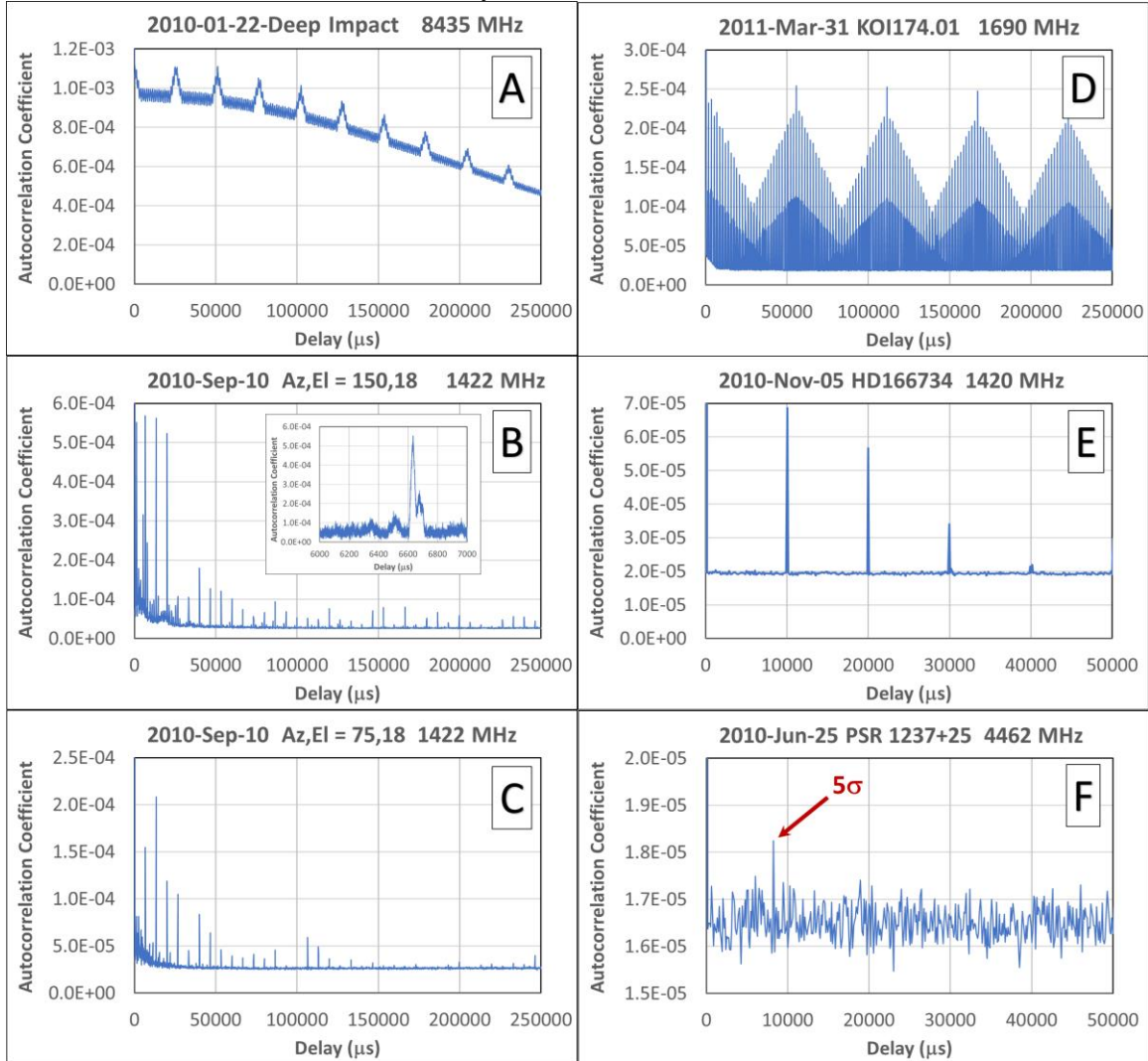


Figure 3: FAC plots of power as a function of delay on various sources. A: The Deep Impact spacecraft in downlink transmission band. B and C: An unexpected interfering signal observed in multiple pointing directions. The inset in B shows a blow up of the delay region around 6500 μ s. D: While pointed at a Kepler object of interest, an observation at 1690 MHz shows signal in the frequency range of Geostationary Operational Environmental Satellites, even though all GOES satellites were far from the pointing direction. E: Observed while pointed at a blue supergiant star, the signal period of 10.000 ms is identified as human-generated due to its close alignment with Earth-based time units. F: While pointed at a pulsar, one of the smallest signals detected in this paper. Although this too is interference, this plot gives an impression of the signal to noise ratio obtained in these measurements.

We estimated the coherence time of the plots B and C signal by computing the statistic using different sample block lengths M but keeping all of the data. The first FAC peak had a maximal plateau for M corresponding to block times greater than 140 ms, while

smaller M resulted in a smaller peak. This plateauing behavior indicates that the repetition period is drifting slowly during the observation, changing by the delay of a single sample ($1.2 \mu s$) in about 140 ms.

The origin of this signal has not been identified nor do we speculate on its origin. This study shows how interfering signals are distinguished from true ETI transmissions using direction-of-arrival estimation. This is important; while some interfering sources can be identified with known transmitters, it is more often the case that the frequencies of such human-generated signals do not correspond with any cataloged source of radiation known to us. Interfering signals are ubiquitous below 5 GHz, and once identified as interference there is no need for further investigation.

The interesting signal in plot D shows how satellite communications can generate interference in FAC observations. We intentionally observed in the transmission band of the GOES weather satellites while pointing far away from any of those satellites. Such strong satellite transmissions make radio observations impossible at frequencies where they occur.

Plot F is provided to highlight the background noise level of all observations. Because the correlations are computed over a finite period, we expect an average autocorrelation coefficient of $\sim 10^{-5}$ even when the input data contain only noise.

Summarizing all the observational results: We found 10 distinct signals in FAC that had no counterparts in PS. At least ten times as many unique signals were observed in the power spectra which indicates that today, interfering signals are more likely to be narrowband than repetitive. All unidentified signals were observed multiple times and in different pointing directions, indicating they arise from terrestrial/satellite communications. No unidentified FAC signal was observed with center frequency above 5 GHz. This indicates very little RFI over the entire upper half of the terrestrial microwave window ($\sim 1-10$ GHz), frequencies where new future SETI observations will be least impacted.

These examples demonstrate a couple of points: 1) FAC is demonstrated to detect repetitive signals that will not be found in a conventional SETI search, and 2) FAC is a good detector for local RFI that may be difficult to characterize otherwise. We do not know of another radio observatory that uses FAC as a means of identifying RFI and we suggest that this approach may be useful elsewhere.

4 Discussion

4.1 Archetypal Signal Motivating This Work

Almost all modes of human communication are fundamentally symbolic with symbols repeating in a complex message. This campaign attempts to find signals containing at least some repetitive periodic structure. An archetypal signal here is the wireless Ethernet protocol. Ethernet uses a binary alphabet of symbols to represent arbitrary information. At the hardware level, each symbol is represented by a particular electromagnetic

waveform in the radio frequency band. Such signals are transmitted and in principle can escape to great distances from the Earth.

A distant astronomer with a radio telescope and sufficient sensitivity can detect the transmitted data stream in a total power measurement. The astronomer sees broadband power arriving from the direction of Earth. Since many natural sources can generate broadband power, the artificial nature of the signal might be overlooked. Alternatively, if she employs a FAC detector then the signal's artificial nature is immediately evident. The FAC detectors are well suited to identify a host of protocols that transmit information using a finite alphabet of symbols. We note that it would be difficult but not impossible to design a symbolic protocol that evades FAC detection.

4.2 Major Conclusions of Campaign

This is a prototype survey and we have learned much about how to effectively mount an expanded and more sensitive SETI campaign for detection of repetitive signals, as discussed below. Now we consider the research question⁹, “What is the highest probability for the existence of true repetitive ETI signal that is compatible with our results?” We emphasize that since this is the first substantial survey looking for constant-power repetitive signals, we have little *a priori* knowledge about this question.

4.2.1 Hypothesis 1

Most previously discovered strong radio sources with flux >1 Jy are modulated with a repeating pattern either directly by extraterrestrials or due to some heretofore unknown physics.

The total population of possible independent observations of all sufficiently strong sources can be estimated as follows. The NVSS survey contains 2206 sources with flux ≥ 1 Jy and declination $> -40^\circ$, corrected to 2690 for the whole sky. The frequency search window, (1-10 GHz) can be divided into 1286 independent 7 MHz ranges as are used here. The number of observations required to perform a complete survey with no overlaps is therefore 3.5×10^6 .

We have 89 independent observations on 23 strong sources, or have performed 2.0×10^{-5} of the complete survey. We assume a uniform distribution of repetitively modulated sources in position and frequency. Given the probability p_+ that a signal will be detected in any one trial, what value of p_+ is consistent with our 89 consecutive observations being negative? We write

$$P = (1 - p_+)^{89} < (2960 * 1286)^{-1}. \quad (5)$$

⁹ A more expansive description of our research hypotheses is given in the Introduction.

This and other probability results are presented in Table 2. We conclude that $p_+ < 0.16$ for this case. That is, we predict a large majority of potential observations on 1 Jy sources will show negative results. Comparatively, a future search with 1500 observations could attain $p_+ < 0.01$.

We reiterate this result including all details: Of the ~ 2690 radio sources in the sky with flux > 1 Jy in the radio frequency range 1-10 GHz, no more than 16% of them might bear (either natural or intentional) repetitive modulation with repeat periods between $1 \times 10^{-4} < \tau < 0.25$ s.

We conclude that our Hypothesis 1 is not supported with no more than one in six sources bearing modulation.

4.2.2 Hypothesis 2

Most bright pulsars with supernova remnants, besides their characteristic repetitive nature, are additionally modulated as above.

According to the ATNF pulsar survey (Manchester et al. 2005) there are 21 pulsars whose integrated flux (at 1400 MHz) is > 1 Jy for a total of 27000 hypothetical 7 MHz observations over the full 1-10 GHz range. This survey made 20 pulsar observations of which 7 were distinct, implying $p_+ < 0.23$.

We conclude that Hypothesis 2 is not supported with no more than one in four pulsars bearing additional modulation.

4.2.3 Hypothesis 3

Out of all the stars in the galaxy, most harbor detectable repetitive transmitters. If these transmitters have a bandwidth that is narrow compared with typical continuum observation bandwidths (> 100 MHz) at some arbitrary frequency, they may not have been discovered in total power observations prior to this study.

We made 88 distinct observations centered on stars. The calculation here is slightly different because a complete survey of all stars at all frequencies is unfeasible. We set up Bayes' relation as in (Harp et al. 2016) and compute the posterior probability distribution π that a new observation will observe a transmitter as

$$\pi(\text{obs} | p_+) = (1 - p_+)^{88}. \quad (6)$$

That is, given a value for p_+ we can compute the likelihood of 88 null observations in a row. To extract concrete information for p_+ , we integrate Equation (6) from $p_+ = 0$ to p_{\max} and set it equal to 0.95. This corresponds to a 95% probability that p_+ lies somewhere in the range $0 \leq p_+ < p_{\max}$. We calculate $p_{\max} = 0.03$ with 95% confidence.

Hypothesis 3 is not supported with no more than one in thirty stars possessing such transmitters.

Table 2:

New Limits on Probability of Repetitive ET Transmitter

Source Type	Num Observations at unique frequencies	Num Sources in Galaxy	p_+
Distinct Source > 1 Jy	31	2690	0.16
Distinct Pulsar	7	21	0.23

Source Type	Num Independent Observations		p_{\max}
Stars	88	10^{11}	0.03

4.2.4 6667 MHz Methanol Masers

Some naturally occurring astronomical sources can be modulated using beams of energy from external sources. Tommy Gold was the first to suggest that this could be done with an astronomical maser, and just such a maser has been found (Weisberg et al. 2005)), albeit the source of modulation was another natural source (pulsar).

We tested two 6667 MHz methanol masers (W3OH and W51) for evidence of repetitive modulation. These masers emit into ~20 kHz wide bands with peak fluxes of 3471 and 850 Jy respectively. Either of these would appear in our survey if they were only 0.03% modulated. There are only 22 such masers in the galaxy. While we cannot draw decisive conclusions from this sample, we can at least say that the strongest methanol masers are not repetitively modulated.

Another result worthy of comment: The L4 Lagrange point showed no evidence for an artifact transmitting repetitive signals in 3 observations at 1420, 2008 and 3991 MHz.

4.3 Number of Signal Waveforms Probed

Matched filter bank detectors can be created for any basis set of signals with known structure. The number of orthogonal functions in a “complete” MFB is equal to the number of sample values or degrees of freedom. For example, a simple M -point narrowband detector (FFT) probes a set of M frequencies, representing the elements of a single basis set. MFB detectors are optimal in terms of having the greatest sensitivity to signals in their basis set.

In principle, one wishes to create MFB detectors for signal types of all kinds, including narrowband, pulsed, chirped, repetitive, and so on. This is computationally expensive. One reasonable approach to generalizing the number of signals detected by an MFB is to give it an extra functional dependence controlled by a free parameter. For example, we can generalize narrowband signals to chirps by allowing

$$\exp(i\omega t) \rightarrow \exp(i(\omega_0 + \omega_1 t)t) \text{ where } \omega_1 = \frac{d\omega}{dt} = \text{const.} \quad (7)$$

is a new variable parameter.

How many different values of ω_1 values are required to fully explore all degrees of freedom in a dataset with M points? The answer is M , if parameter values are chosen to make all the resulting MFB basis functions orthogonal. Often, exact orthogonality is difficult to arrange, but the right number of parameter values to test is always of order M . In this paper, we shall call two MFBs with distinct parameter values as being sensitive to two different “types” of signals.

The time to compute a one or two parameter MFB is typically M or M^2 times longer, respectively, than the time to compute an MFB with no parameters. Due to computational constraints, typical MFBs in SETI are generalized with no more than two parameterized variables¹⁰. This is a relatively small number when compared to the number of signal types probed by FAC.

Classic and recent theoretical studies of the interstellar medium as a communication channel (Drake 1965; Messerschmitt 2012; Messerschmitt & Morrison 2012; Shostak 1995) suggest algorithms capable of discovering radio signals that contain information, a good example being autocorrelation detection (Drake 1965; Harp et al. 2010a; Jones 1995). Autocorrelation is sensitive to signals having *arbitrary* message content provided some part of the signal repeats with duration $2 \leq n_{rep} \leq \frac{M}{4}$ where n_{rep} is the repeat period

in samples (demanding at least four repeats during observation as in this paper; n_{rep} need not be an integer). Consider the example of a binary symbol alphabet. The total number of signal waveforms probed by FAC in a single analysis is of order

$\left(2^{\frac{M}{4}} + 2^{\frac{M-1}{4}} + 2^{\frac{M-2}{4}} \dots + 2 \right)$ and dramatically outnumbers the types probed by an MFB with two free parameters.

In this work, the observations block size $M = 2^{23}$ complex samples corresponding to ~ 1 second duration. Extending the above example, just for binary encodings and one possible repeated message length $\frac{M}{4}$, this analysis will discover any of $2^{21} \approx 10^{630000}$

different¹¹ possible wide-bandwidth waveforms. This is compared to $M^3 \approx 10^{21}$ different signals for a fully-sampled two parameter MFB on the same data. Including all possible repeat lengths and all possible symbol encodings, FAC probes a practically infinite number of signal types with only a fraction of the computational requirements of a two

¹⁰ Here we speak of SETI studies where the MFB is applied in real time as the data are acquired. Offline computations, obviously, have no such constraint.

¹¹ By “different” we mean that there is this many orthogonal functions tested.

dimensional matched filter search (e.g. about twice the computation for a spectral power search (Harp et al. 2010a)).

This impressive advantage of FAC SETI is offset by the fact that a stronger transmitter power is required to excite an FAC detector as compared with a MFB. We discuss the interplay of variables in the next section. We shall conclude that FAC searches are best when the source flux exceeds the equivalent flux of the telescope and sky noise over the integration time.

4.4 Figure of Merit

As a basis for discussion, we consider the figure of merit (FOM) $N_{\text{Trans}} N_{\text{Types}}$ described above.¹² This FOM takes into account only the two variables relevant to this discussion, and other plausible FOMs could be constructed. For example, a different FOM might attach another functional dependence to the number of signal types probed, creating a different ranking of detector comparisons.

If the telescope is pointed in a direction with weak radio flux, then the extra sensitivity of a matched filter is traded off against the limited signal types probed. Far from the transmitter, an electromagnetic signal decreases in areal power density as R^{-2} , where R is the radius from the transmitter. For a given a transmitter power P_t , and assuming a uniform distribution of transmitters in space, the radial reach of a signals energy scales as $P_t^{3/2}$. Comparatively, FAC detection falls off as R^{-4} and the transmitter reach varies as P_t^3 .

For this campaign, the MFB detection threshold is 0.009 Jy as compared to 0.037 Jy for FAC (Table 1). The ratio of the number of transmitters probed by the matched filter to the number probed by FAC is therefore $(0.185/0.045)^{3/2} = 8$. Referencing the discussion in section 4.3, the figure of merit $N_{\text{Stars}} N_{\text{Types}}$ dramatically favors FAC searches over any two parameter MFB.

It may be true that somehow, the spectrally pure signal (sinusoid) is strongly favored by builders of ET transmitters over any other signal type. FAC is not at all sensitive to such beacons and the traditional SETI narrowband search is the optimal. However, there are some down sides to sinusoidal signals. The first is that a pure sinusoid carries only one bit of information: that a transmitter exists. Furthermore, it has been argued (Messerschmitt 2012) that sinusoidal signals are less resistant to RFI and multipath (time variable scintillation-induced) fading than say, a spread spectrum signal that is repetitively modulated. In this case a narrowband filter will be relatively insensitive to the

¹² N_{Trans} is the number of transmitters in a spherical volume that are probed for a given sensitivity and N_{Types} is the number of signal types probed.

signal, yet FAC will be. One last argument against sinusoidal beacons is that most Earth-based radio communications are rapidly converging on spread spectrum signals.

4.5 Comparison to KLT

We believe that in the future, most MFB and FAC searches will be overtaken by a signal detector based on principle component (a.k.a. eigenvector, a.k.a. singular value) decomposition and detection of received signals. In SETI signal processing literature, principle component decomposition is referred to as the Karhunen–Loève Transform (KLT), which renders a set of equal length multi-dimensional vectors (e.g. blocks of a time series) into a power-ordered expansion of orthogonal eigenvectors.

The promise of KLT is that an arbitrary (repeating) signal waveform in the presence of Gaussian noise can be detected with a sensitivity close to that of a MFB, provided one chooses to compare observation blocks with a period commensurate with the repeat period. One promising implementation of KLT for SETI is the so-called BAM-KLT (Maccone 2010). For illustration we consider a simplified version of this algorithm.

Assume an observation with N_s samples comprising Gaussian noise plus an arbitrary signal from an ET transmitter. We suppose the transmitted signal has a repetitive structure with repeat length l_{rep} samples (not necessarily an integer).

The N_s samples are arranged in blocks forming the rows of a $N_b \times M$. The eigenvectors are ordered by eigenvalue, and only a small number of eigenvectors need be computed requiring $O(N_s^2)$ operations (can use Lanczos algorithm to efficiently determine first few eigenvectors). If M is sufficiently close to l_{rep} , then the eigenvector with the largest eigenvalue is a good approximation of the transmitted signal waveform. We don't know the value of l_{rep} ; it is necessary to repeat this process for all values $2 < M < N_s / 4$. So a complete BAM-KLT computation scales as $O(N_s^3)$.

By comparison FAC detection on the same signal requires $O(N_s \ln(N_s))$ operations. For the campaign presented here, BAM-KLT would require approximately 10^{11} times more processing than FAC. Despite this computational barrier, we are confident that some KLT variant will eventually prevail in SETI searches since it is optimal for the problem and the computations are highly parallelizable.

4.6 An Improved FAC Search Design for the Future

We have shown that FAC detection probes an immense region of signal discovery space not observed in conventional SETI campaigns. In designing the next generation search we consider two target types: 1) Search for repetition in radiation from known strong sources, and 2) Search for repetitive signals from directions where no strong flux is expected.

Targets having known flux should be chosen such that they carry sufficient flux to trigger FAC detection. The minimum detectable flux in this paper is ~ 1 Jy which is well above the threshold for FAC at the ATA. The Very Large Array archives contain measurements on all the brightest sources above -20 degrees declination. If the raw correlator data are available, a substantial search for repetitive signals from many more bright sources is possible.

For targets not showing up in previous radio surveys we infer they do not show substantial flux over very wide bandwidths (~ 100 MHz), but they may show flux over modest bandwidths (Hz to 10's of MHz) not previously detected. An examination of Table 1 shows that such sources would be more easily discovered using a total power imaging survey than with direct application of FAC processing. This is because the sensitivity to raw power is greater than the sensitivity to FAC.

From these considerations, we propose the next generation SETI detection system should include 3 components. 1) A total power imaging survey covering all frequencies between 1-10 GHz. 2) A conventional narrowband SETI detector. 3) An autocorrelation detector running in parallel and even using the same data streams as for 1) and 2).

4.7 Computation of FAC from Correlator Output

FAC can be applied to any observed power spectral data. And besides single-dish or phased array beam data, we believe we are the first to point out that radio interferometer data for imaging can be an excellent source of data for archival FAC searches. Large archives of untested data are available from many telescopes, including the VLA, Westerbork, SRT, GMRT, MeerKat, and ASKAP at centimeter wavelengths; LOFAR and other low frequency arrays; and at high frequencies with ALMA.

Most interferometers designed for radio imaging employ FX correlators where antenna data is first Fourier transformed (F) followed by cross correlation of every antenna with every other antenna (X) to give spectral visibilities. Visibilities are integrated over time periods typically from seconds to minutes, and then stored for subsequent image generation. FX correlator datasets are well suited for FAC because a delay spectrum can be computed from each of hundreds to thousands of correlation spectra. RFI rejection can be implemented by comparing delay spectra across all antenna pairs, since for a point source in the field of view, a repetitive ET signal should have the same FAC in every correlation, whereas RFI coming from outside the field of view will not be constant across correlations. After this step, these delay spectra can be combined (coherently or incoherently) to give a time-dependent delay spectrum sensitive to the entire field of view.

With only modest resources, we can undertake a rich research program covering essentially the whole sky by applying this new style of SETI analysis on archival interferometer data. We demonstrate this approach using archival data from a joint experiment between the ATA and the Arecibo Observatory Figure 4. The Arecibo planetary radar was pointed toward the center of the Moon, and transmissions using binary phase-shift keying (BPSK) were sent with a transmitter bandwidth of 27 MHz. The chip (symbol) duration was $0.5 \mu\text{s}$ and the same string of 63 symbols was sent over

and over. The signal had no amplitude modulation (only phase) with a repetition rate of 31.5 μs .

The ATA was pointed toward the Moon with a field of view much larger than the Moon's diameter. Arecibo transmitted at 2380 MHz with 250 kW of power. Neglecting specular reflection we assume that this power was 100%¹³ diffusely scattered into a hemisphere, and taking into account the distance between Earth and Moon, the proportion arriving in the ATA was less than 10^{-7} of the transmitted signal. The ATA filling factor is less than 1%, so the signal entering our array aperture was about 2.5×10^{-7} W; it was so strong that it was difficult to attenuate the signal enough to prevent overdriving the receivers.

Because the radar is circularly polarized, choosing different polarizations on antenna pairs (XY or YX, cross-polarization) captures the reflected polarized signal (shown) and isolating the radar signal from background radiation. XX, YY spectra (not shown for brevity) showed very similar features. Visibility spectra from the Moon-bounce observation were Fourier transformed to the delay domain and then summed coherently. Clear peaks are seen in Figure 4, with delays corresponding to the 31.5 μs repeat time of the transmitted BPSK signal.

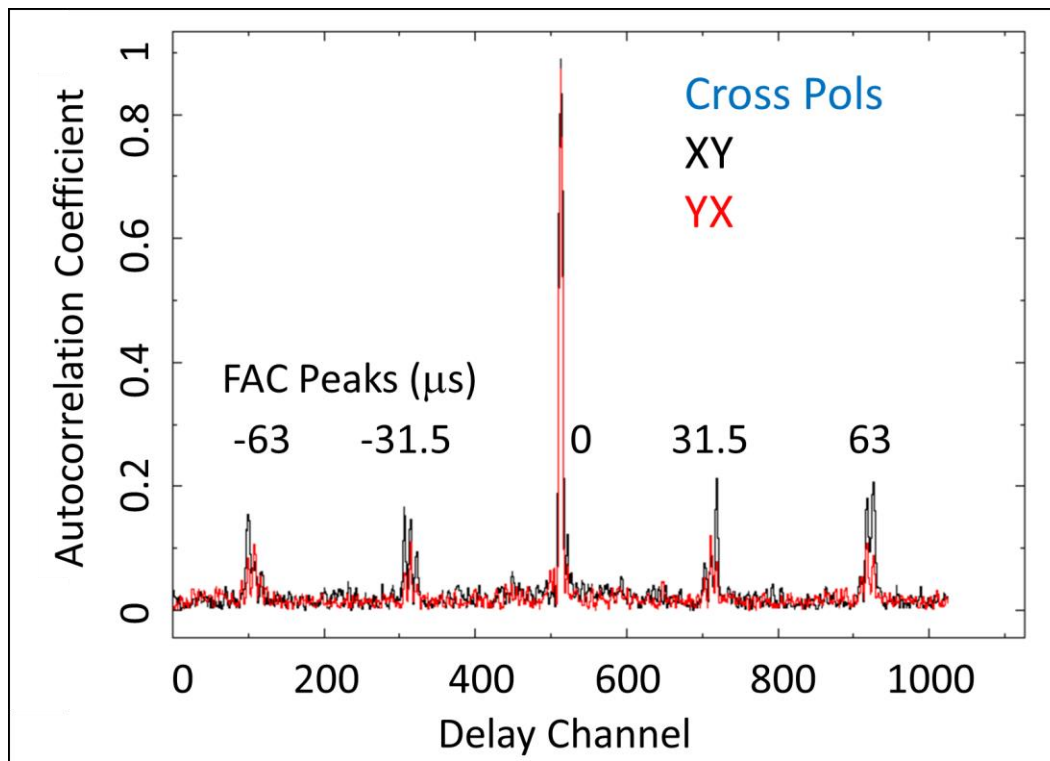


Figure 4: Demonstration of the FAC technique using an imaging correlator as detector. Since most modern interferometer telescopes use correlators, this method has wide application.

¹³ The true reflectivity is about 10% of this.

Compared to the 2×10^6 delay values examined in this survey, FAC observations with a correlator are limited in delay. The ATA correlator has a fixed number of 1024 spectral bins independent of the spectral bandwidth. Thus, no more than 512 delay values may be observed. Since correlators generally integrate over periods measured in seconds (possibly ms periods in the next generation), we are limited to a maximum delay equal to half the inverse bin width. At the ATA, the maximum delay values for 104 MHz to 6.5 MHz settings are $4.8 \mu\text{s}$ to $77 \mu\text{s}$, respectively. Hence FAC signal searches are optimized when using the maximum number of channels in the correlator, and different delay ranges can be covered with different correlator observation bandwidths.

4.8 Beyond Detection of FAC Signals

The relationship between artificial repetition and real sky structure in correlator images deserves further comment. When a point source is within the field of view (FOV), it generally appears as regular oscillations or fringes within the visibility bandwidth for every antenna pair.¹⁴ The fringe period versus frequency depends on the orientation and distance between the antenna pair (baseline), and it is stationary on all baselines when the interferometer is phased up on the source. We call these *structure fringes* because they originate from source structure in the field of view.

Repetitive sources introduce what we call *delay fringes* into the visibility spectra. Unless mitigated, delay fringes generate spurious structure in the radio image. Unlike structure fringes, delay fringes have the same oscillation period versus frequency in every visibility, independent of the antenna positions. The latter property allows us to distinguish real spatial structure from signal repetition.

Structure fringes show peaks in the delay domain, one for each point source in the image. Sources at phase center peak at zero delay. Sources far from phase center exhibit peaks with a range of positive or negative delays on different baselines.

In comparison, if a repetitive signal (from anywhere) is present, then FAC peaks will appear at the same delay values for all baselines. Because delay fringes transform to a range of differently scaled structure in images, artificial repetitive signals may generate telescope-specific and time-dependent “halos” around the phase center.

Summing delay fringes over baselines reinforces repetition delay peaks relative to structural delay peaks, at once providing a robust detection scheme for identifying artificial repetitive signals. If these signals are unwanted, their interference peaks may be zeroed out in delay spectra after which a Fourier transform back to the frequency domain can result in improved imaging.

¹⁴ For discussion, assume the source bandwidth is greater than observation bandwidth.

5 Conclusions

This paper reports a novel survey of galactic and extra-galactic targets (quasars, supernova remnants, masers, pulsars, stars with known planets, O-type stars, the Lagrange L4 point, etc.) searching for artificially engineered signals bearing repetitive structure. Signal detection was performed using ~10 minute observations with 7 MHz effective bandwidth captured to disk and post-processed using autocorrelation of the complex-valued voltage signal.

The scientific outcomes of this survey include:

1. We put an upper limit on the number of continuum sources that are artificially modulated with repetitive signals. For sources with flux >1 Jy, no more than 16% are repetitively modulated.
2. For pulsars and supernova remnants whose combined flux is >1 Jy, no more than 23% are artificially modulated.
3. For stars at a 95% confidence level, no more than 3% contain undiscovered signals with repetitive modulation and flux greater than 0.3 Jy.
4. Neither of the two strongest methanol masers in the galaxy show evidence for repetitive modulation down to a level of 0.03% of the maser flux.
5. No unexpected, repetitive transmissions with flux >0.3 Jy appear to be arriving from the Earth-Sun L4 Lagrange point near 1420, 2008 and 3991 MHz.

When a new probe for extraterrestrial signals is introduced, even a modest survey can add greatly to the human reservoir of knowledge. This paper reports the first search for repetitive extraterrestrial signals, some of which might be hiding “in plain sight” but not detected in ordinary analyses of radio telescope data. This principle is demonstrated by the discovery of heretofore unknown and strong repetitive RFI at the ATA.

We were able to eliminate all observed repetitive signals as candidates for an extraterrestrial signal using direction of origin methods alone and without prior knowledge of human transmitters’ frequencies or physical locations. This is generally true for all the SETI performed at the SETI Institute, with the exception of a relatively small number of signals that disappear before their direction of origin can be determined. There were no such cases in the present work.

Finally, we lay the groundwork for a proposed campaign to look for repetitive signals using archived correlator data, especially on known sources with continuum flux at several times the noise floor of the telescope. Such a campaign requires no new observations and can explore all of the sky over a modest range of repetition delays.

Acknowledgements

The authors gratefully acknowledge Franklin P. Antonio for support of this research.

6 Appendix

6.1 Details of Digital Computation

The actual numerical calculations of PS, FAC and IAC are rather more complex than the notional equations (2), (3) and (4). For all statistics, the initial Fourier transform is performed on a block of $M = 2^{22}$ samples corresponding to one-half second in time. Prior to FFT the block is shifted to zero mean to eliminate the uninteresting zero frequency feature. The block is then multiplied by a Hanning window. This is a raised cosine function that goes to zero at the edges of the sampled time, and removes many artifacts present in a simple periodogram. After the first block, the latter $M/2$ samples from the first block is retained and concatenated with $M/2$ new samples from the dataset. In conjunction with the Hanning window, this overlapping preserves the total power of the sampled data after FFT.

For PS and FAC, we use the sampled electric field values as the starting point for the FFT. After the first FFT, the transformed values are squared to compute the power spectrum (PS). For FAC, the averaged power spectrum is padded with $M/2$ zeros on each end to form an array of length $2M$. This padding prevents mixing of positive and negative delays. The result is passed through an inverse FFT (Weiner-Kinchin theorem) to find the complex-valued autocorrelation statistic. When the signal is stationary, the complex-valued statistic can be averaged over long times. However, this is not always the case (see discussion of Figure 3A and B). To minimize cancellation to the extent possible, we average the absolute value of the FAC statistic over one-half second intervals, hence it is real and positive definite at all points with units of power.

As computed, correlation statistics are biased with a smoothly-varying envelope, peaking at zero delay and going to zero at maximum delay. We correct (normalize) for this bias by dividing each FAC coefficient by the coefficient for a signal containing pure Gaussian noise over a very long time ($\gg 10$ minutes) and subjected to the same analysis. Although this normalization introduces mild heteroscedasticity, we focus our attention on only the lower 50% of delay values to minimize its effects.

The raw autocorrelation values in the plots of Figure 3 have 2^{21} individual points, much more than can be adequately displayed in a printed plot. To bring the number of points down to a manageable group, the original AC data are binned with a max-pooling method (each point represents the largest of 1024 points in the raw AC data). To give a better impression of the actual point density we blow up a region around the first peak in Figure 3B which includes all the computed AC values between 6000 and 7000 microseconds.

The convolution algorithm (Wiener–Khinchin theorem) for FAC is important in this application as it costs only 2x more computation than for the PS (Harp et al. 2010a). A more sensitive FAC-based algorithm, symbol-wise autocorrelation (Morrison 2012, 2017) might be pursued in future studies but will require $>400,000$ times more computation time than for the campaign presented here.

Bibliography

- Ackermann, R. F., & Harp, G. R. 2012, 3,
http://wiki.setiquest.info/index.php/SetiQuest_Data_Links.
- Barott, W. C., Milgrome, O., Wright, M., et al. 2011, *Radio Sci*, 46, RS1016
- Boyd, R. W., & Werner, M. W. 1972, *Astrophys J*, 174, L137
- Cocconi, G., & Morrison, P. 1959, *Nature*, 184, 844,
http://www.iaragroup.org/_OLD/seti/pdf_IARA/cocconi.pdf
- Cordes, J. M. 2002, in *ASP Conference Series: Single-Dish Radio Astronomy: Techniques and Applications*, Vol. 278,
<http://adsabs.harvard.edu/full/2002ASPC..278..227C>
- Drake, F. D. 1961, *Phys Today*, 40
- Drake, F. D. 1965, in *Current Aspects of Exobiology*, 323
- Eaton, J. W., Bateman, D., & Hauberg, S. 1997, *Gnu Octave. A high-level interactive language for numerical computations* (Boston, MA: Free Software Foundation),
<http://folk.ntnu.no/joern/itgk/octave.pdf>
- Fano, R. M. 1951, *Signal-To-Noise Ratio in Correlation Detectors* (Technical Report No. 186) No. NP-3081., Technical Report 186, Research Lab. of Electronics, Mass. Inst. of Tech., 1951.
- Gardner, W. A., & Spooner, C. M. 1992, *IEEE Trans Commun*, 40, 149
- Harp, G. R., Ackermann, R. F., Blair, S. K., et al. 2010a, in *Communication with Extraterrestrial Intelligence*, ed. D. A. Vakoch (SUNY Press), 45,
http://www.amazon.com/Communication-Extraterrestrial-Intelligence-Douglas-Vakoch/dp/1438437943/ref=sr_1_1?ie=UTF8&s=books&qid=1304639895&sr=1-1
- Harp, G. R., Ackermann, R. F., Nadler, Z. J., et al. 2011, *IEEE Antennas Propagation*, 59, 2004
- Harp, G. R., Ackermann, R. F., Olsen, E., & Bhatt, A. 2010b, *SetiQuest Wiki*,
http://setiquest.org/wiki/index.php/SetiQuest_Data_Links
- Harp, G. R., Richards, J., Tarter, J. C., et al. 2016, *Ap J*, 152, 181,
<http://arxiv.org/abs/1607.04207>
- Jones, H. W. 1995, in *Progress in the Search for Extraterrestrial Life*, V. 74, ed. G. S. Shostak, http://articles.adsabs.harvard.edu/cgi-bin/nph-iarticle_query?1995ASPC...74..369J&defaultprint=YES&filetype=.pdf
- Von Korff, J., Demorest, P., Heien, E., et al. 2013, *Ap J*, 767, 40
- Korpela, B. E., Werthimer, D., Anderson, D., Cobb, J., & Lebofsky, M. 2001, *Comput Sci Eng*, 3, 78
- Leeb, W. R., Alves, J., Meingast, S., & Brunner, M. 2015, *Astron Astrophys*, 574, A9,
<http://www.aanda.org/10.1051/0004-6361/201424480>
- Leshem, A., van der Veen, A., Boonstra, A., van der Veen, J., & Boonstra, A. 2000, *Astrophys J Suppl Ser*, 131, 355, <http://stacks.iop.org/0067-0049/131/i=1/a=355>

- Maccone, C. 2010, *Acta Astronaut*, 67, 1427,
<http://linkinghub.elsevier.com/retrieve/pii/S0094576510001487>
- Manchester, R., Hobbs, G., Teoh, A., & Hobbs, M. 2005, *Ap J*, 129, 1993
- McQuillan, A., Mazeh, T., & Aigrain, S. 2014, *Astrophys J Suppl Ser*, 211, 24,
<http://arxiv.org/abs/1402.5694>[http://labs.adsabs.harvard.edu/adsabs/abs/2014ApJS.
.211...24M/](http://labs.adsabs.harvard.edu/adsabs/abs/2014ApJS..211...24M/)
- Messerschmitt, D. G. 2012, *Acta Astronaut*, 81, 227
- Messerschmitt, D. G., & Morrison, I. S. 2012, *Acta Astronaut*, 78, 80
- Morrison, I. S. 2011, *ATA Memo Ser*, 93, 1
- Morrison, I. S. 2012, *Acta Astronaut*, 78 (Elsevier), 90,
<http://www.sciencedirect.com/science/article/pii/S0094576511003092>
- Morrison, I. S. 2017, *Constraining the discovery space for artificial interstellar signals* (University of New South Wales),
http://www.unsworks.unsw.edu.au/primolibweb/action/dlDisplay.do?vid=UNSWORKS&docId=unsworks_46149
- Oliver, B. M., & Billingham, J. 1971, 1971 NASA/ASEE Summer Fac Fellowsh Progr (NASA-CR-114445), 1 (Palo Alto, CA),
http://ntrs.nasa.gov/archive/nasa/casi.ntrs.nasa.gov/19730010095_1973010095.pdf
- Rickett, B. J., Kedziora-Chudczer, L., & Jauncey, D. L. 2002, *ApJ*, 581, 103,
<http://adsabs.harvard.edu/abs/2002ApJ...581..103R>
- Shostak, G. S. 1995, in *Progress in the Search for Extraterrestrial Life*, A.S.P. Conference Series, 74, ed. G. S. Shostak, 447,
<http://articles.adsabs.harvard.edu/full/1995ASPC...74..447S>
- Shuch, H. P. 2011, *Searching for Extraterrestrial Intelligence: SETI Past, Present, and Future* (Berlin Heidelberg: Springer)
- Siemion, A., Von Korff, J., McMahon, P., et al. 2010, *Acta Astronaut*, 67, 1342
- Tarter, J. C. 2001, *Annu Rev Astron Astrophys*, 39, 511
- Tarter, J. C., Agrawal, A., Ackermann, R., et al. 2010, *SPIE Opt Eng Appl*, 7819, 781902
- Wayth, R. B., Brisken, W. F., Deller, A. T., et al. 2011, *Astrophys J*, 735, 97,
<http://arxiv.org/abs/1104.4908>
- Weisberg, J. M., Johnston, S., Koribalski, B., & Stanimirovic, S. 2005, *Science*, 309, 106,
<http://www.ncbi.nlm.nih.gov/pubmed/15919955>
- Welch, J., Backer, D., Blitz, L., et al. 2009, *Proc IEEE*, 97, 1438,
<http://arxiv.org/pdf/0904.0762>
- Wozencraft, J. M., & Jacobs, I. M. 1990, *Principles of Communication Engineering* (Prospect Heights, IL: Waveland Press, Inc.)

6.2 Appendix: Observation Table

List of all observations collected for this project. The raw data for these observations are available online (Harp et al. 2010b). Sources with “off” in their name track the path of the stated object but following the real source with a delay of ~ 1 hr.

Table 3:

List of Observations for This Study

Source	Coordinate	Type	Freq (MHz)	Flux (Jy) @obs freq	Date
0136+478	01 36 59 +47 51 29	quasar	2008	1.7	2010-12-24
0136+478	01 36 59 +47 51 29	quasar	4462	1.9	2010-12-17
0136+478	01 36 59 +47 51 29	quasar	6670	1.9	2010-12-12
0228+673	02 28 50 +67 21 03	quasar	2008	1.2	2011-01-07
0228+673	02 28 50 +67 21 03	quasar	6670	2.0	2010-12-12
0744-064	07 44 22 -06 29 36	quasar	2840	4.7	2010-07-02
0834+555	08 34 55 +55 34 21	quasar	2840	6.8	2010-07-02
0834+555	08 34 55 +55 34 21	quasar	2840	6.8	2010-12-24
0834+555	08 34 55 +55 34 21	quasar	3100	6.6	2010-07-22
0834+555	08 34 55 +55 34 21	quasar	6670	4.4	2010-12-17
1347+122	13 47 33 +12 17 24	quasar	2008	4.6	2010-12-24
1347+122	13 47 33 +12 17 24	quasar	4462	3.0	2010-12-24
1347+122	13 47 33 +12 17 24	quasar	6670	2.7	2010-12-12
1733-130	17 33 03 -13 04 50	quasar	2008	5.1	2011-02-04
1733-130	17 33 03 -13 04 50	quasar	4462	4.8	2010-12-17
1733-130	17 33 03 -13 04 50	quasar	6670	10.1	2010-12-12
2038+513	20 38 37 +51 19 13	quasar	2008	4.9	2011-02-04
2038+513	20 38 37 +51 19 13	quasar	6670	3.4	2010-12-17
2206-185	22 06 10 -18 35 39	quasar	2008	5.8	2011-02-04
2206-185	22 06 10 -18 35 39	quasar	4462	3.9	2010-12-17
3c119	04 32 37 +41 38 28	quasar	2008	7.1	2011-02-04
3c119	04 32 37 +41 38 28	quasar	2840	5.4	2010-07-02
3c119	04 32 37 +41 38 28	quasar	4462	3.9	2010-06-25
3c123	04 37 04 +29 40 14	quasar	2008	39.7	2011-02-04
3c123	04 37 04 +29 40 14	quasar	2840	31.7	2010-07-02
3c123	04 37 04 +29 40 14	quasar	4465	23.6	2010-06-25
3c138	05 21 10 +16 38 22	quasar	2008	7.1	2011-02-04
3c138	05 21 10 +16 38 22	quasar	2840	5.4	2010-07-02
3c138	05 21 10 +16 38 22	quasar	4462	4.0	2010-06-25
3c147	05 42 36 +49 51 07	quasar	2008	18.1	2011-02-04
3c147	05 42 36 +49 51 07	quasar	2840	12.5	2010-07-02
3c147	05 42 36 +49 51 07	quasar	4462	8.6	2010-06-25
3c274	12 30 49 +12 23 29	quasar	2008	3.0	2010-12-24

3c274	12 30 49 +12 23 29	quasar	2840	3.0	2010-07-02
3c274	12 30 49 +12 23 29	quasar	4462	3.0	2010-12-24
3c274	12 30 49 +12 23 29	quasar	6670	3.0	2010-12-17
3c279	12 56 11 -05 47 22	quasar	6670	13.6	2010-12-17
3c286	13 31 08 +30 30 33	quasar	1420	14.9	2010-10-15
3c286	13 31 08 +30 30 33	quasar	2008	12.9	2011-01-07
3c286	13 31 08 +30 30 33	quasar	2008	12.9	2010-12-24
3c286	13 31 08 +30 30 33	quasar	4020	8.4	2010-10-08
3c286	13 31 08 +30 30 33	quasar	6670	6.3	2010-12-12
3c295	14 11 21 +52 12 09	quasar	2008	17.0	2011-01-07
3c295	14 11 21 +52 12 09	quasar	6670	3.0	2010-12-12
3c345	16 42 59 +39 48 37	quasar	2008	7.9	2011-01-07
3c345	16 42 59 +39 48 37	quasar	2008	7.9	2011-02-04
3c345	16 42 59 +39 48 37	quasar	6670	5.5	2010-12-12
3c380	18 29 32 +48 44 46	quasar	2008	10.6	2011-02-04
3c380	18 29 32 +48 44 46	quasar	6670	4.0	2010-12-17
3c395	19 02 56 +31 59 42	quasar	6670	1.2	2010-12-17
3c48	01 37 41 +33 09 35	quasar	1422	16.5	2010-08-13
3c48	01 37 41 +33 09 35	quasar	2008	13.0	2010-12-24
3c48	01 37 41 +33 09 35	quasar	2840	8.9	2010-07-02
3c48	01 37 41 +33 09 35	quasar	4462	5.9	2010-12-17
3c48	01 37 41 +33 09 35	quasar	6670	4.2	2010-12-24
3c84	03 19 48 +41 30 42	quasar	2840	23.6	2010-07-02
3c84	03 19 48 +41 30 42	quasar	4462	23.4	2010-06-25
3c84	03 19 48 +41 30 42	quasar	4462	23.4	2010-09-10
3c84	03 19 48 +41 30 42	quasar	6670	22.1	2010-12-17

Blazars						
BLlacterus	22 02 43 +42 16 40	blazar	1420	6.1	2010-10-15	
BLlacterus	22 02 43 +42 16 40	blazar	2008	5.9	2010-10-15	
BLlacterus	22 02 43 +42 16 40	blazar	6670	4.2	2010-05-21	
BLlacterus	22 02 43 +42 16 40	blazar	8200	4.0	2010-08-13	
S5 0716+714	07 21 53 +71 20 36	blazar	1414	~1.5 varies	2010-10-15	
S5 0716+714	07 21 53 +71 20 36	blazar	1420	~1.5 varies	2010-10-15	
S5 0716+714	07 21 53 +71 20 36	blazar	1420	~1.5 varies	2010-05-21	
S5 0716+714	07 21 53 +71 20 36	blazar	1422	~1.5 varies	2010-08-13	
S5 0716+714	07 21 53 +71 20 36	blazar	1422	~1.5 varies	2010-08-13	
S5 0716+714	07 21 53 +71 20 36	blazar	1422	~1.5 varies	2010-10-15	
S5 0716+714	07 21 53 +71 20 36	blazar	1426	~1.5 varies	2010-08-13	
S5 0716+714	07 21 53 +71 20 36	blazar	1427	~1.5 varies	2010-10-15	
S5 0716+714	07 21 53 +71 20 36	blazar	1432	~1.5 varies	2010-08-13	
S5 0716+714	07 21 53 +71 20 36	blazar	1435	~1.5 varies	2010-05-21	
S5 0716+714	07 21 53 +71 20 36	blazar	1459	~1.5 varies	2010-10-22	
S5 0716+714	07 21 53 +71 20 36	blazar	3086	~1.5 varies	2010-12-17	
S5 0716+714	07 21 53 +71 20 36	blazar	6670	~1.5 varies	2010-10-22	
S5 0716+714	07 21 53 +71 20 36	blazar	8200	~1.5 varies	2010-05-07	

0954+658	09 58 47 +65 33 55	blazar	1432	~1.3 varies	2010-10-15
0954+658	09 58 47 +65 33 55	blazar	8200	~1.3 varies	2010-10-22

Supernova Remnants and Masers

taua	05 34 32 +22 00 58	SNR	2008	1110.0	2010-08-13
taua	05 34 32 +22 00 58	SNR	1420	1110.0	2010-05-07
taua	05 34 32 +22 00 58	SNR	2840	1110.0	2010-10-15
casa	23 23 27 +58 48 28	SNR	2008	1547.3	2010-08-13
casa	23 23 27 +58 48 28	SNR	4462	885.9	2010-10-15
casa	23 23 27 +58 48 28	SNR	6670	701.1	2010-08-13
w51	19 23 44 +14 30 33	maser	6670	850 peak	2010-05-07
w3oh	02 27 04 +61 52 25	maser	6670	3741 peak	2010-03-26
w3oh	02 27 04 +61 52 25	maser	6670	3741 peak	2010-04-02
w3oh	02 27 04 +61 52 25	maser	6670	3741 peak	2010-05-07

Pulsars @1400 MHz

crab	05 34 32 +22 00 52	pulsar	2008	12.6	2011-02-04
crab	05 34 32 +22 00 52	pulsar	1420	12.6	2010-03-26
crab	05 34 32 +22 00 52	pulsar	1420	12.6	2010-10-15
crab	05 34 32 +22 00 52	pulsar	2600	12.6	2010-03-09
crab	05 34 32 +22 00 52	pulsar	4462	12.6	2010-05-07
crab	05 34 32 +22 00 52	pulsar	1420	12.6	2010-05-07
crab	05 34 32 +22 00 52	pulsar	4462	12.6	2010-06-25
psrb0329+54	03 32 59 +54 34 44	pulsar	1420	1.8	2010-05-07
psrb0329+54	03 32 59 +54 34 44	pulsar	1420	1.8	2010-05-21
psrb0329+54	03 32 59 +54 34 44	pulsar	611	1.8	2011-03-04
psrb0450+55	04 54 08 +55 43 42	pulsar	4462	0.3	2010-06-25
psrb0809+74	08 14 59 +74 29 06	pulsar	4462	0.0	2010-06-25
psrb0809+74	08 14 59 +74 29 06	pulsar	1420	0.0	2010-05-14
psrb0823+26	08 26 51 +26 37 24	pulsar	4462	0.1	2010-06-18
psrb0823+26	08 26 51 +26 37 24	pulsar	4462	0.1	2010-06-25
psrb0950+08	09 53 09 +07 55 36	pulsar	4462	3.2	2010-06-18
psrb0950+08	09 53 09 +07 55 36	pulsar	4462	3.2	2010-06-25
psrb1133+16	11 36 03 +15 51 04	pulsar	4462	0.9	2010-06-25
psrb1237+25	12 39 40 +24 53 49	pulsar	4462	0.4	2010-06-25
psrb1937+21	19 39 39 +21 34 59	pulsar	1420	0.3	2010-11-05

Stars - Including Kepler Exoplanets, O-stars

koi001	13 12 44 -31 52 24	exoplanet	4462	<1	2010-09-10
koi044	22 53 13 -14 15 13	exoplanet	4462	<1	2010-03-26
koi051	09 34 50 -12 07 46	exoplanet	4462	<1	2010-09-10
koi054	10 58 28 -10 46 13	exoplanet	4462	<1	2010-09-10
koi060	03 32 55 -09 27 29	exoplanet	1420	<1	2010-03-19
koi062	12 44 20 -08 40 17	exoplanet	4462	<1	2010-09-10
koi071	11 35 52 -04 45 21	exoplanet	4462	<1	2010-09-10
koi072	22 09 40 -04 38 27	exoplanet	4462	<1	2010-03-26
koi073	09 56 06 -03 48 30	exoplanet	4462	<1	2010-09-10

koi076	12 19 13 -03 19 11	exoplanet	4462	<1	2010-09-10
koi080	13 12 43 -02 15 54	exoplanet	4462	<1	2010-09-10
koi081	10 42 48 -02 11 01	exoplanet	4462	<1	2010-09-10
koi084	11 24 17 -01 31 44	exoplanet	4462	<1	2010-09-10
koi096	11 45 42 +02 49 17	exoplanet	4462	<1	2010-09-10
koi097	11 26 46 +03 00 22	exoplanet	4462	<1	2010-09-10
koi112	12 13 29 +10 02 29	exoplanet	4462	<1	2010-09-10
koi117	10 18 21 +12 37 15	exoplanet	4462	<1	2010-09-10
koi118	13 28 26 +13 47 12	exoplanet	4462	<1	2010-09-10
koi119	11 46 24 +14 07 26	exoplanet	4462	<1	2010-09-10
koi125	13 12 19 +17 31 01	exoplanet	4462	<1	2010-09-10
koi126	10 10 07 +18 11 12	exoplanet	4462	<1	2010-09-10
koi127	23 18 47 +18 38 45	exoplanet	3100	<1	2010-07-22
koi130	04 42 56 +18 57 29	exoplanet	1420	<1	2010-03-19
koi133	09 23 47 +20 21 52	exoplanet	3100	<1	2010-07-22
koi134	00 44 41 +20 26 56	exoplanet	4462	<1	2010-03-26
koi144	00 39 21 +21 15 01	exoplanet	1420	<1	2010-03-19
koi150	02 04 34 +25 24 51	exoplanet	4462	<1	2010-03-26
koi155	11 42 11 +26 42 23	exoplanet	4462	<1	2010-09-10
koi160	08 52 37 +28 20 02	exoplanet	1420	<1	2010-03-19
koi172	00 20 40 +31 59 24	exoplanet	4462	<1	2010-03-26
koi191	22 57 47 +38 40 30	exoplanet	3100	<1	2010-07-22
koi195	10 59 29 +40 25 46	exoplanet	4462	<1	2010-09-10
koi201	10 22 10 +41 13 46	exoplanet	4462	<1	2010-09-10
koi201	10 22 10 +41 13 46	exoplanet	3100	<1	2010-07-22
koi202	01 36 48 +41 24 38	exoplanet	1420	<1	2010-03-19
koi208	06 04 29 +44 15 37	exoplanet	3100	<1	2010-07-22
koi211	19 28 59 +47 58 10	exoplanet	1420	<1	2010-09-24
koi211	19 28 59 +47 58 10	exoplanet	4462	<1	2010-10-01
koi216	07 48 07 +50 13 33	exoplanet	3100	<1	2010-07-22
koi219	14 56 55 +53 22 56	exoplanet	1420	<1	2010-09-24
koi219	14 56 55 +53 22 56	exoplanet	4462	<1	2010-10-01
koi220	13 34 02 +53 43 42	exoplanet	4462	<1	2010-09-10
koi221	15 35 16 +53 55 20	exoplanet	1420	<1	2010-09-24
koi221	15 35 16 +53 55 20	exoplanet	4462	<1	2010-10-01
koi222	18 10 32 +54 17 12	exoplanet	4462	<1	2010-10-01
koi225	07 21 33 +58 16 05	exoplanet	4462	<1	2010-10-01
koi226	15 24 55 +58 57 57	exoplanet	4462	<1	2010-10-01
koi227	08 18 22 +61 27 38	exoplanet	4462	<1	2010-10-01
koi228	08 40 13 +64 19 41	exoplanet	4462	<1	2010-10-01
koi231	12 05 15 +76 54 20	exoplanet	4462	<1	2010-09-10
koi233	05 22 33 +79 13 52	exoplanet	3100	<1	2010-07-22
koi236	13 00 03 +12 00 07	exoplanet	4462	<1	2010-09-10
Gliese581	15 19 27 -07 43 20	exoplanet	1420	<1	2010-10-01
Gliese581	15 19 27 -07 43 20	exoplanet	4462	<1	2011-01-28

Gliese581	15 19 27 -07 43 20	exoplanet	4462	<1	2010-10-01
koi04	19 02 28 +50 08 09	exoplanet	1418	<1	2010-05-14
koi04	19 02 28 +50 08 09	exoplanet	1420	<1	2010-01-22
koi04	19 02 28 +50 08 09	exoplanet	1420	<1	2010-03-19
koi04	19 02 28 +50 08 09	exoplanet	1420	<1	2010-03-19
koi04	19 02 28 +50 08 09	exoplanet	1420	<1	2010-04-02
koi04	19 02 28 +50 08 09	exoplanet	1420	<1	2010-09-24
koi04	19 02 28 +50 08 09	exoplanet	1420	<1	2010-11-05
koi04	19 02 28 +50 08 09	exoplanet	1420	<1	2010-05-14
koi04	19 02 28 +50 08 09	exoplanet	1692	<1	2010-09-24
koi139.01	19 26 37 +44 41 18	exoplanet	1690	<1	2011-03-31
koi174.01	19 47 18 +48 06 27	exoplanet	1690	<1	2011-03-31
koi268.01	19 02 55 +38 30 25	exoplanet	1690	<1	2011-03-31
koi51.01	19 43 40 +41 19 57	exoplanet	1690	<1	2011-03-31
koi70.03	19 10 48 +42 20 19	exoplanet	1690	<1	2011-03-31
55Cncr1	08 52 36 +28 19 51	OZMA star	1420	<1	2010-11-05
zetaOph	16 37 10 -10 34 02	O-star	1420	<1	2010-11-05
zetaOph	16 37 10 -10 34 02	O-star	2008	<1	2010-12-24
zetaOph	16 37 10 -10 34 02	O-star	2840	<1	2010-12-24
zetaOph	16 37 10 -10 34 02	O-star	6670	<1	2010-12-17
HD172175	18 39 04 -07 51 35	O-star	1420	<1	2010-11-05
HD166734	18 12 25 -10 43 53	O-star	1420	<1	2010-11-05
HD093521	10 48 24 +37 34 13	O-star	1420	<1	2010-11-05
HD060848	07 37 06 +16 54 15	O-star	1420	<1	2010-11-05
BD114586	18 18 03 -11 17 39	O-star	1420	<1	2010-11-05
Special Pointings					
Sun	N/A	Sun	1414	~1000000	2010-10-15
Sun	N/A	Sun	1420	~1000000	2010-10-15
Sun	N/A	Sun	1426	~1000000	2010-10-15
Moon	N/A	Moon	1420	~10000	2010-10-08
Moon	N/A	Moon	1420	~10000	2010-11-05
northpole	00 00 00 +90 00 00	North Pole	1543	<1	2010-10-22
northpole	00 00 00 +90 00 00	North Pole	3086	<1	2010-10-22
Lagrange-4	Sun-Earth L4	Lagrange point	1420	<1	2010-10-08
Lagrange-4	Sun-Earth L4	Lagrange point	2008	<1	2010-10-08
Lagrange-4	Sun-Earth L4	Lagrange point	3991	<1	2010-10-08
galanticenter	05 45 37 +28 56 10	Galactic Anticenter	1420	<1	2010-05-07
galanticenter	05 45 37 +28 56 10	Galactic Anticenter	1422	<1	2010-05-07
galanticenter	05 45 37 +28 56 10	Galactic Anticenter	3991	<1	2010-05-07

		Galactic			
galanticenter	05 45 37 +28 56 10	Anticenter	3991	<1	2010-10-08
		Galactic			
galanticenter	05 45 37 +28 56 10	Anticenter	4462	<1	2010-05-07
		Galactic			
galanticenter	05 45 37 +28 56 10	Anticenter	2008	<1	2010-05-07
		Galactic			
galanticenter	05 45 37 +28 56 10	Anticenter	3991	<1	2010-10-08

Confirmation Observations (intentionally away from some particular source)

blank06	06 00 00 +40 00 00	off beam	1422		?
blank06	06 00 00 +40 00 00	off beam	1427		?
blank18	18 00 00 +70 00 00	off beam	6670		?
blank18	18 00 00 +70 00 00	off beam	2008		?
blank	09 18 06 -11 54 17	off beam	2840		?
off	03 32 56 +09 27 30	off beam	1420		?
EpsilonEridani					
off EtaAreitis	02 12 48 +21 12 39	off beam	1420		?
off	05 45 37 +33 56 10	off beam	2008		?
galanticenter					
off	05 45 37 +33 56 10	off beam	3991		?
galanticenter					
off Gliese581	15 19 27 +07 43 20	off beam	4462		?
off Gliese581	15 19 27 +07 43 20	off beam	1420		?
off HD69830	08 18 24 +12 37 56	off beam	1420		?
off TauCeti	01 44 04 +15 56 15	off beam	1420		?

Confirmation Observations (surveying RFI at ATA)

AZEL360-18	fixed az, el	Az sweep	1410		?
AZEL345-18	fixed az, el	Az sweep	1410		?
AZEL330-18	fixed az, el	Az sweep	1410		?
AZEL315-18	fixed az, el	Az sweep	1410		?
AZEL300-18	fixed az, el	Az sweep	1410		?
AZEL285-18	fixed az, el	Az sweep	1410		?
AZEL270-18	fixed az, el	Az sweep	1410		?
AZEL255-18	fixed az, el	Az sweep	1410		?
AZEL240-18	fixed az, el	Az sweep	1410		?
AZEL225-18	fixed az, el	Az sweep	1410		?
AZEL210-18	fixed az, el	Az sweep	1410		?
AZEL195-18	fixed az, el	Az sweep	1410		?
AZEL180-18	fixed az, el	Az sweep	1410		?
AZEL165-18	fixed az, el	Az sweep	1410		?
AZEL150-18	fixed az, el	Az sweep	1410		?
AZEL135-18	fixed az, el	Az sweep	1410		?
AZEL120-18	fixed az, el	Az sweep	1410		?
AZEL105-18	fixed az, el	Az sweep	1410		?
AZEL090-18	fixed az, el	Az sweep	1410		?
AZEL075-18	fixed az, el	Az sweep	1410		?

AZEL060-18	fixed az, el	Az sweep	1410	?
AZEL045-18	fixed az, el	Az sweep	1410	?
AZEL030-18	fixed az, el	Az sweep	1410	?
AZEL015-18	fixed az, el	Az sweep	1410	?

